

Electronic Supplementary Information

Enhancing the Performance of Ionic Conductivity for Solid-state Electrolyte: An Effective Strategy of Injecting Lithium Ions within Anionic Metal–Organic Frameworks

Lu Shi, Xin Wang and Zhiliang Liu*

Inner Mongolia Key Laboratory of Chemistry and Physics of Rare Earth Materials,
College of Chemistry and Chemical Engineering, Inner Mongolia University, Hohhot
010021, P. R. China.

E-mail: cezliu@imu.edu.cn.

Fax/Tel: +86–471–4992922

Contents

Experimental Section

Electrochemical Measurements

Fig. S1 SEM images of (a) $(\text{CH}_3)_2\text{NH}_2^+[\text{Cu-BTC}]^-$ and (b) $\text{Li}^+[\text{Cu-BTC}]^-$.

Fig. S2 XRD patterns of $(\text{CH}_3)_2\text{NH}_2^+[\text{Cu-BTC}]^-$ and $\text{Li}^+[\text{Cu-BTC}]^-$.

Fig. S3 TGA curves of $(\text{CH}_3)_2\text{NH}_2^+[\text{Cu-BTC}]^-$ and $\text{Li}^+[\text{Cu-BTC}]^-$ in N_2 atmosphere.

Fig. S4 FT-IR spectra of $(\text{CH}_3)_2\text{NH}_2^+[\text{Cu-BTC}]^-$ and $\text{Li}^+[\text{Cu-BTC}]^-$.

Fig. S5 (a) N_2 adsorption and desorption isotherms and (b) pore size distribution of $(\text{CH}_3)_2\text{NH}_2^+[\text{Cu-BTC}]^-$ and $\text{Li}^+[\text{Cu-BTC}]^-$.

Fig. S6 Nyquist plots of (a) $(\text{CH}_3)_2\text{NH}_2^+[\text{Cu-BTC}]^-$ and (b) $\text{Li}^+[\text{Cu-BTC}]^-$ at various temperatures.

Fig. S7 Current-time curve of (a) $\text{Li}||(\text{CH}_3)_2\text{NH}_2^+[\text{Cu-BTC}]^-||\text{Li}$ cells and (b) $\text{Li}||\text{Li}^+[\text{Cu-BTC}]^-||\text{Li}$ cells (the inset is EIS before and after polarization).

Fig. S8 EIS spectra of $\text{Li}||(\text{CH}_3)_2\text{NH}_2^+[\text{Cu-BTC}]^-||\text{Li}$ and $\text{Li}||\text{Li}^+[\text{Cu-BTC}]^-||\text{Li}$ cells at -20°C .

Fig. S9 SEM images of Li foil for Li symmetric cells with (a) $(\text{CH}_3)_2\text{NH}_2^+[\text{Cu-BTC}]^-$, (b) $\text{Li}^+[\text{Cu-BTC}]^-$ after 500 h cycles. Schematic diagrams of the Li deposition behavior with (c) $(\text{CH}_3)_2\text{NH}_2^+[\text{Cu-BTC}]^-$, (d) $\text{Li}^+[\text{Cu-BTC}]^-$.

Fig. S10 XRD pattern of $\text{Li}^+[\text{Cu-BTC}]^-$ after galvanostatic charge and discharge cycling.

Table S1 ICP results of $\text{Li}^+[\text{Cu-BTC}]^-$.

Table S2 Surface area and pore volume of $(\text{CH}_3)_2\text{NH}_2^+[\text{Cu-BTC}]^-$ and (d) $\text{Li}^+[\text{Cu-BTC}]^-$.

Table S3 Ionic conductivity of $(\text{CH}_3)_2\text{NH}_2^+[\text{Cu-BTC}]^-$ and (d) $\text{Li}^+[\text{Cu-BTC}]^-$ at various temperatures.

Table S4 Summary of ionic conductivity of different solid-state electrolytes in high and low temperatures.

Table S5 Comparison of the ionic conductivity and Li^+ transference number of different MOFs-based solid-state electrolytes.

References

Experimental Section

Materials

All chemicals and reagents were used as received without additional purification: copper(II) chloride dihydrate ($\text{CuCl}_2 \cdot 2\text{H}_2\text{O}$, 99%), 1,3,5-benzentricarboxylic acid (BTC, 98%), lithium nitrate (LiNO_3 , 99%), ethanol ($\geq 99.7\%$), methanol ($\geq 99.5\%$) *N,N*-dimethylformamide (DMF, $\geq 99.5\%$), *N,N*-dimethylacetamide (DMA, $\geq 99.5\%$), 1M LiPF_6 in ethylene carbonate/diethyl carbonate (EC/DEC, 1:1 vol%), isopropyl alcohol ($\geq 99.7\%$), polyvinylidene fluoride (PVDF, 99%), poly(tetrafluoroethylene) (PTFE, 60%), *N*-methyl-2-pyrrolidone (NMP, 98.0%), acetylene black, LiFePO_4 , CR2032 coin cell components and aluminum foil (Al foil, 99.9%).

Synthesis

Synthesis of $(\text{CH}_3)_2\text{NH}_2^+[\text{Cu-BTC}]^-$.¹ The anionic Cu-BTC was synthesized according to a previously reported with minor modification. Typically, 13 mmol $\text{CuCl}_2 \cdot 2\text{H}_2\text{O}$ and 6.5 mmol BTC were dissolved in a solution of DMA under magnetic stirring. Then the mixture was heated at 100°C for 48 h. The precipitates were washed with DMF and ethanol, followed by drying at 80°C for 12 h.

Synthesis of $\text{Li}^+[\text{Cu-BTC}]^-$. 100 mg $(\text{CH}_3)_2\text{NH}_2^+[\text{Cu-BTC}]^-$ crystals were dispersed in 20 mL of 0.5 M methanol solution of LiNO_3 at room temperature. The solution was changed two times per day over three days. The product was washed with fresh methanol several times, and dried at 80°C for 12 h.

Preparation of solid-state electrolyte membranes. MOF powders were homogeneously dispersed in isopropanol and 10% PTFE aqueous solution. After continuous grinding and volatilization of the solvent, the mixture was rolled into electrolyte membranes. The membranes were cut into flexible pieces with a diameter of 16 mm and a thickness of 0.28 mm, and dried at 80°C overnight. Then the electrolyte membranes were stored in a glove box and soaked in 1 M LiPF_6 solution for 24 h. The excess liquid electrolyte was wiped with filter paper.

Preparation of cathode material. The LiFePO_4 cathode materials were prepared by coating NMP-based slurry including 80 wt% LiFePO_4 powders, 10 wt% PVDF and 10% acetylene black onto an aluminum foil. After drying at 120°C for 8 h, the electrode

film was cut into sheets with a thickness of 200 μm and a diameter of 16 mm. The loading of LiFePO_4 was about 2–3 mg cm^{-2} .

Materials characterization

Powder X-ray diffraction (PXRD) measurement was recorded on an Empyrean PANalytical diffractometer with $\text{Cu K}\alpha$ radiation ($\lambda = 1.5406 \text{ \AA}$) at 40 mA and 40 kV. Scanning electron microscopy (SEM) images were obtained using a Hitachi S-4800 Scanning electron microscopy. Brunauer-Emmett-Teller surface area and pore structure were determined using Micromeritics ASPS 2460 at 77 K. Thermogravimetric analysis (TGA) was performed on a NETZSCH TG 209F3 with a heating rate of $10 \text{ }^\circ\text{C min}^{-1}$ under a nitrogen atmosphere. Inductively coupled plasma optical emission spectroscopy (ICP-OES) was measured using an Agilent 720. Fourier-transform infrared spectroscopy (FTIR) spectra were collected by an IRTRACER-100.

Electrochemical Measurements

Ionic conductivity was measured using electrochemical impedance spectroscopy after placing the solid-state electrolytes between two stainless-steel blocking electrodes (SS|electrolyte|SS) in a CR2032 coin cell. The frequency range was from 10^6 to 1 Hz with an amplitude of 5 mV, and the measurement temperature range was $-40^\circ\text{C}\sim 100^\circ\text{C}$. Ionic conductivity (σ , S cm^{-1}) was calculated by equation (1):

$$\sigma = \frac{L}{R \times S} \quad (1)$$

where L , R and S are the thickness, bulk resistance and area of the electrolyte, respectively.

The activation energy (E_a) was obtained based on the Arrhenius equation (2):

$$\sigma = A e^{(-E_a/RT)} \quad (2)$$

where A is the pre-exponential factor, and T is the Kelvin temperature.

Lithium ions transference number (t_{Li^+}) was measured through AC impedance and potentiostatic polarization measurements using Li|electrolyte|Li cells. The t_{Li^+} was calculated by equation (3):

$$t_{Li^+} = \frac{I_{ss}(\Delta V - I_0 R_0)}{I_0(\Delta V - I_{ss} R_{ss})} \quad (3)$$

where ΔV is the polarization voltage (10 mV), I_0 and I_{ss} are the initial and stable-state currents, R_0 and R_{ss} are the resistance before and after polarization, respectively.

Electrochemical stability window was obtained by linear sweep voltammetry (LSV) in a Li|electrolyte|SS asymmetric cell with a scan rate of 1 mV s⁻¹.

The lithium stripping/plating behavior was carried out by charging and discharging using a Li|electrolyte|Li cell at 0.1 mA cm⁻². The rate performance was measured using LiFePO₄|electrolyte|Li cells at 0.1~2.0 C (1 C = 170 mA g⁻¹). The cycling ability and charge-discharge capacity were evaluated using LiFePO₄|electrolyte|Li cells at 0.1 C between 2.5 and 4.2 V on a LANDCT2001A testing system.

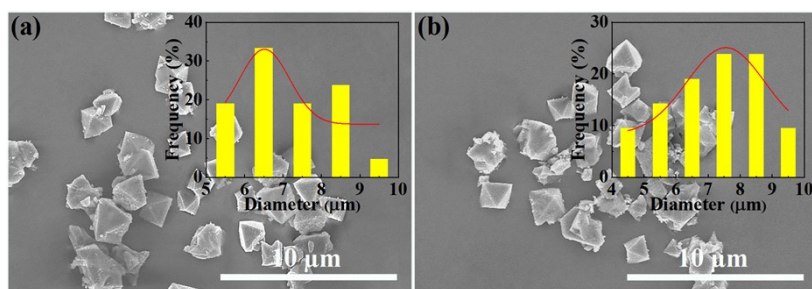


Fig. S1 SEM images of (a) $(\text{CH}_3)_2\text{NH}_2^+[\text{Cu-BTC}]^-$, and (b) $\text{Li}^+[\text{Cu-BTC}]^-$.

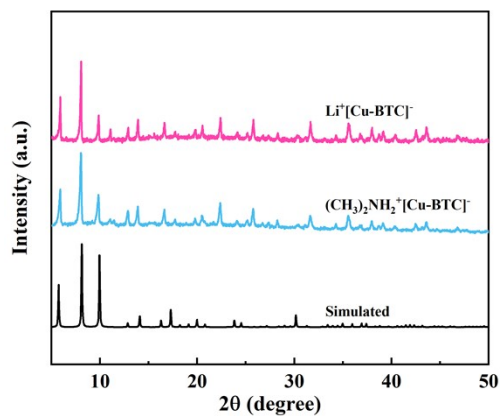


Fig. S2 XRD patterns of $(\text{CH}_3)_2\text{NH}_2^+[\text{Cu-BTC}]^-$ and $\text{Li}^+[\text{Cu-BTC}]^-$.

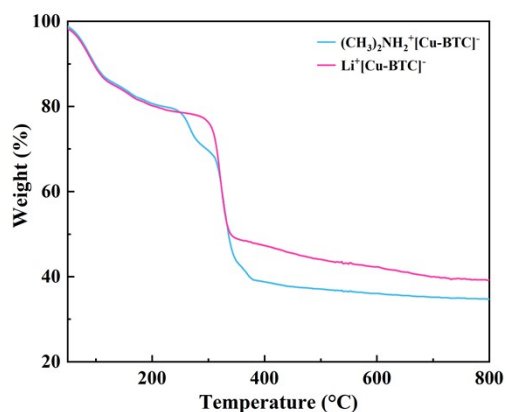


Fig. S3 TGA curves of $(\text{CH}_3)_2\text{NH}_2^+[\text{Cu-BTC}]^-$ and $\text{Li}^+[\text{Cu-BTC}]^-$ in N_2 atmosphere.

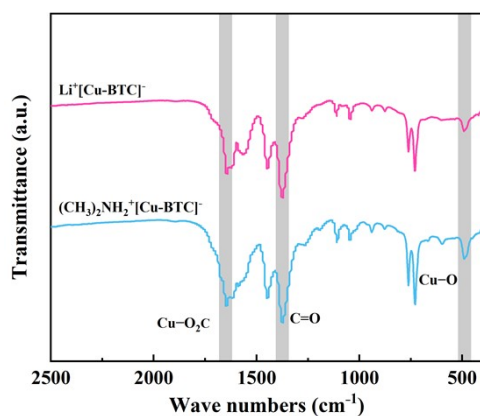


Fig. S4 FT-IR spectra of $(\text{CH}_3)_2\text{NH}_2^+[\text{Cu-BTC}]^-$ and $\text{Li}^+[\text{Cu-BTC}]^-$.

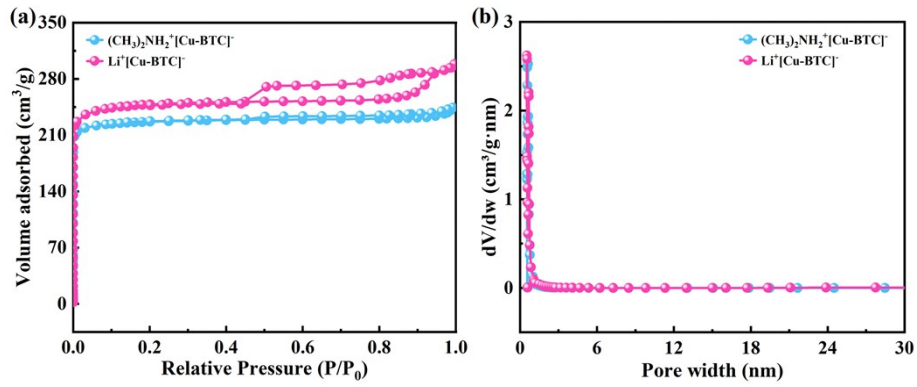


Fig. S5 (a) N_2 adsorption and desorption isotherms and (b) pore size distribution of $(\text{CH}_3)_2\text{NH}_2^+[\text{Cu-BTC}]^-$ and $\text{Li}^+[\text{Cu-BTC}]^-$.

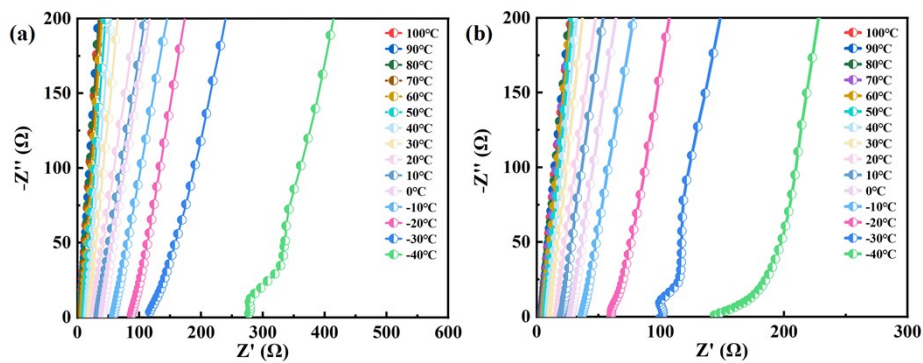


Fig. S6 Nyquist plots of (a) $(\text{CH}_3)_2\text{NH}_2^+[\text{Cu-BTC}]^-$ and (b) $\text{Li}^+[\text{Cu-BTC}]^-$ at various temperatures.

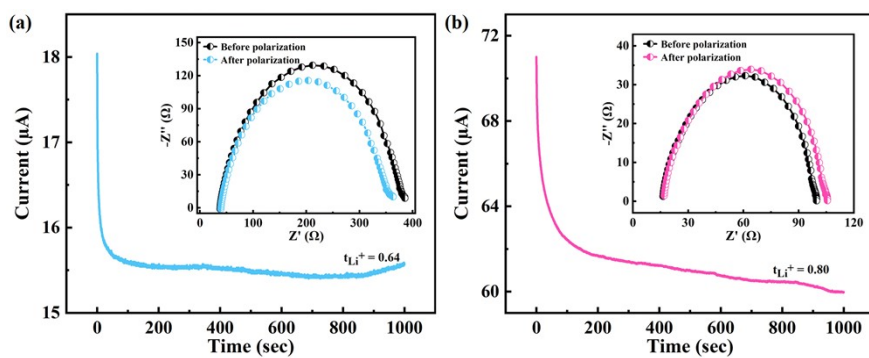


Fig. S7 Current-time curve of (a) $\text{Li}[(\text{CH}_3)_2\text{NH}_2^+[\text{Cu-BTC}]^-]|\text{Li}$ cells and (b) $\text{Li}|\text{Li}^+[\text{Cu-BTC}]^-|\text{Li}$ cells (the inset is EIS before and after polarization).

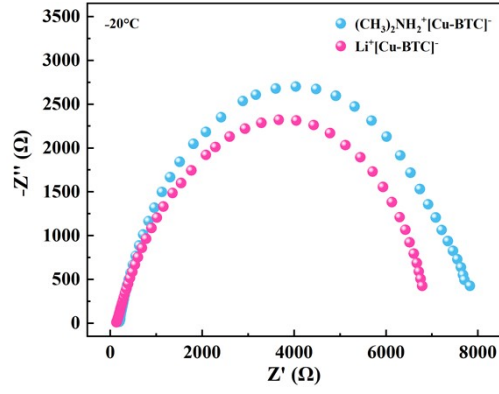


Fig. S8 EIS spectra of Li|(CH₃)₂NH₂⁺[Cu-BTC]⁻|Li and Li|Li⁺[Cu-BTC]⁻|Li cells at -20°C.

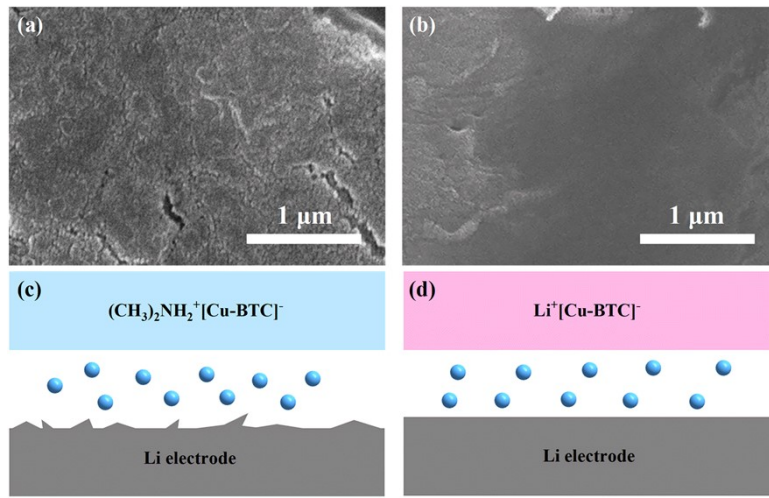


Fig. S9 SEM images of Li foil for Li symmetric cells with (a) (CH₃)₂NH₂⁺[Cu-BTC]⁻, (b) Li⁺[Cu-BTC]⁻ after 500 h cycles. Schematic diagrams of the Li deposition behavior with (c) (CH₃)₂NH₂⁺[Cu-BTC]⁻, (d) Li⁺[Cu-BTC]⁻.

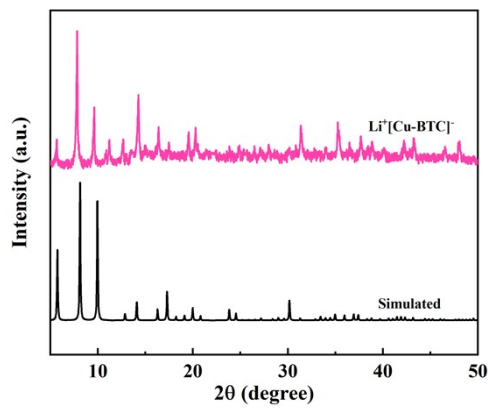


Fig. S10 XRD pattern of Li⁺[Cu-BTC]⁻ after galvanostatic charge and discharge cycling.

Table S1 ICP results of Li⁺[Cu-BTC]⁻.

Samples	Cu	Li	Li/Cu molar ratio
Li ⁺ [Cu-BTC] ⁻	16.58%	0.56%	0.31

Table S2 Surface area and pore volume of (CH₃)₂NH₂⁺[Cu-BTC]⁻ and Li⁺[Cu-BTC]⁻.

Samples	BET surface area (m ² g ⁻¹)	Total pore volume (cm ³ g ⁻¹)	Micropore pore size (nm)
(CH ₃) ₂ NH ₂ ⁺ [Cu-BTC] ⁻	926.17	0.306	0.63
Li ⁺ [Cu-BTC] ⁻	986.45	0.383	0.68

Table S3 Ionic conductivity of (CH₃)₂NH₂⁺[Cu-BTC]⁻ and Li⁺[Cu-BTC]⁻ at various temperatures.

Temperature (°C)	σ (S cm ⁻¹)	
	(CH ₃) ₂ NH ₂ ⁺ [Cu-BTC] ⁻	Li ⁺ [Cu-BTC] ⁻
100	2.02×10 ⁻³	2.96×10 ⁻³
90	1.80×10 ⁻³	2.72×10 ⁻³
80	1.57×10 ⁻³	2.45×10 ⁻³
70	1.33×10 ⁻³	2.18×10 ⁻³
60	1.09×10 ⁻³	1.88×10 ⁻³
50	8.62×10 ⁻⁴	1.58×10 ⁻³
40	6.67×10 ⁻⁴	1.29×10 ⁻³
30	5.21×10 ⁻⁴	1.19×10 ⁻³
20	4.16×10 ⁻⁴	1.12×10 ⁻³
10	3.24×10 ⁻⁴	6.25×10 ⁻⁴
0	2.68×10 ⁻⁴	4.55×10 ⁻⁴
-10	1.80×10 ⁻⁴	3.41×10 ⁻⁴
-20	1.17×10 ⁻⁴	2.05×10 ⁻⁴
-30	8.04×10 ⁻⁵	1.23×10 ⁻⁴
-40	3.88×10 ⁻⁵	1.10×10 ⁻⁴

Table S4 Summary of ionic conductivity of different solid-state electrolytes in high and low temperatures.

Materials	σ (S cm ⁻¹)	Temperature (°C)	Ref.
PESF-LLZTO CPEs	9.42×10^{-4}	80	S2
	1.49×10^{-4}	-10	
1,3,5-trioxane-based polymer	2.20×10^{-4}	-20	S3
Hollow ZIF-8	1.97×10^{-3}	100	S4
	2.46×10^{-4}	-20	
ZIF-67@ZIF-8	4.89×10^{-3}	100	S5
	3.44×10^{-4}	-20	
MOF-525	4.90×10^{-3}	100	S6
	2.2×10^{-5}	-20	
BStSi	2.20×10^{-3}	100	S7
	3.10×10^{-5}	-20	
NUST-23	1.36×10^{-3}	80	S8
	9.74×10^{-7}	-40	
SE-PMOF	3.31×10^{-3}	60	S9
	1.62×10^{-4}	-20	
LCMOF-1	1.43×10^{-3}	60	S10
	3.45×10^{-5}	-20	
TPB-DMTP-COF	2.10×10^{-5}	-30	S11
LiCON-3	1.17×10^{-4}	100	S12
	0.90×10^{-5}	-40	
Li ⁺ [Cu-BTC] ⁻	2.96×10^{-3}	100	This work
	1.10×10^{-4}	-40	

Table S5 Comparison of the ionic conductivity and Li⁺ transference number of different MOFs-based solid-state electrolytes.

Materials	σ (S cm ⁻¹)	t_{Li^+}	Ref.
UiO-66-NH ₂ @67	9.73×10^{-5}	0.67	S13
MOF-BZN	8.76×10^{-4}	0.75	S14
MOF-SN-FEC	7.04×10^{-4}	0.68	S15
Zr-MA-Li	6.62×10^{-4}	0.63	S16
SIL/UiO-66	2.20×10^{-4}	0.35	S17
Al-MOF	2.00×10^{-4}	0.84	S18
SN-ZIF-69	1.37×10^{-4}	0.67	S19
Li-IL@MOF	3.43×10^{-4}	0.29	S20
Hollow UiO-66	1.15×10^{-3}	0.70	S21
Li-Cuboct-H	1.02×10^{-3}	0.56	S22
Li ⁺ [Cu-BTC] ⁻	1.16×10^{-3}	0.80	This work

References

1. Y.X. Tan, Y.P. He and J. Zhang, *Chem. Commun.*, 2011, **47**, 10647–10649.
2. J. Sun, M. Tian, H. Dong, Z. Lu, L. Peng, Y. Rong, R. Yang, J. Shu and C. Jin, *Appl. Mater. Today*, 2022, **27**, 101447.
3. Z. Li, R. Yu, S. Weng, Q. Zhang, X. Wang and X. Guo, *Nat. Commun.*, 2023, **14**, 482.
4. L. Tian, Z. Liu, F. Tao, M. Liu and Z. Liu, *Dalton Trans.*, 2021, **50**, 13877–13882.
5. Z. Liu, P. Liu, L. Tian, J. Xiao, R. Cui and Z. Liu, *Chem. Commun.*, 2020, **56**, 14629–14632.
6. Z. Wang, R. Tan, H. Wang, L. Yang, J. Hu, H. Chen and F. Pan, *Adv. Mater.*, 2017, **30**, 1704436.
7. Z. Lin and J. Liu, *RSC Adv.*, 2019, **9**, 34601–34606.
8. Y. Xuan, Y. Wang, B. He, S. Bian, J. Liu, B. Xu and G. Zhang, *Chem. Mater.*, 2022, **34**, 9104–9110.
9. Q. Zhang, B. Liu, J. Wang, Q. Li, D. Li, S. Guo, Y. Xiao, Q. Zeng, W. He, M. Zheng, Y. Ma and S. Huang, *ACS Energy Lett.*, 2020, **5**, 2919–2926.
10. Q. Zhang, D. Li, J. Wang, S. Guo, W. Zhang, D. Chen, Q. Li, X. Rui, L. Gan and S. Huang, *Nanoscale*, 2020, **12**, 6976–6982.
11. J. Wang, L. Liu, Y. Liu, X. M. Zhang and J. Li, *Small*, 2023, **19**, 2207831.
12. X. Li, Q. Hou, W. Huang, H.-S. Xu, X. Wang, W. Yu, R. Li, K. Zhang, L. Wang, Z. Chen, K. Xie and K. P. Loh, *ACS Energy Lett.*, 2020, **5**, 3498–3506.
13. Q. Zhang, S. Wang, Y. Liu, M. Wang, R. Chen, Z. Zhu, X. Qiu, S. Xu and T. Wei, *Energy Technol.*, 2023, **11**, 2201438.
14. Y. Ouyang, W. Gong, Q. Zhang, J. Wang, S. J. Guo, Y. B. Xiao, D. X. Li, C. H. Wang, X. L. Sun, C. Y. Wang and S. M. Huang, *Adv. Mater.*, 2023, **35**, 2304685.
15. D. D. Han, P. F. Wang, P. Li, J. Shi, J. Liu, P. J. Chen, L. P. Zhai, L. W. Mi and Y. Z. Fu, *ACS Appl. Mater. Inter.*, 2021, **13**, 52688–52696.
16. Q. Zhang, Y. Xiao, Q. Li, J. Wang, S. Guo, X. Li, Y. Ouyang, Q. Zeng, W. He and S. Huang, *Dalton Trans.*, 2021, **50**, 2928–2935.
17. Z. Liu, Z. Hu, X. Jiang, X. Wang, Z. Li, Z. Chen, Y. Zhang and S. Zhang, *Small*, 2022, **18**, 2203011.
18. W.X. Liu, X.C. Huang, Y. Meng, D. Xiao and Y. Guo, *J. Mater. Chem. A*, 2023, **11**, 13446–13458.
19. X. Zhu, Z. Chang, H. Yang, P. He and H. Zhou, *J. Mater. Chem. A*, 2022, **10**, 651–663.
20. Z. Wu, Y. Yi, F. Hai, X. Tian, S. Zheng, J. Guo, W. Tang, W. Hua and M. Li, *ACS Appl. Mater. Inter.*, 2023, **15**, 22065–22074.
21. Z. X. Liu, W. Z. Chen, F. L. Zhang, F. Wu, R. J. Chen and L. Li, *Small*, 2023, **19**, 2206655.
22. H. L. Liu, H. G. Pan, M. Yan, X. Zhang and Y. Z. Jiang, *Adv. Mater.*, 2023, **35**, 2300888.